Dendritic growth in a mean-field lattice gas model

Mathis Plapp* and Jean-François Gouyet†
Laboratoire de Physique de la Matière Condensée, Ecole Polytechnique, 91128 Palaiseau, France
(Received 18 April 1996)

We study a stochastic lattice gas model with attractive nearest-neighbor interaction. In a mean-field approximation, its local master equation can be written as a generalized Cahn-Hilliard equation. Numerical simulations in two dimensions show the growth of regular snowflakes. Our microscopic equation of motion naturally shows curvature and kinetic effects at the interface as assumed by the classic phenomenological equations of dendritic growth. In addition, we find solute trapping. The dendrite tips are stabilized by the Gibbs-Thomson boundary condition. We calculate the surface tension and show that it has the expected angular variation. Some numerical results for the kinetic coefficient are given. We compare our model to other microscopic growth models and the phase-field models, and discuss the influence of noise. [S1063-651X(96)01912-5]

PACS number(s): 05.70.Ln, 68.70.+w, 05.50.+q, 68.35.Md

I. INTRODUCTION

Phenomena of dendritic growth have been a challenging subject for theorists for a long time and are an active field of research. The spontaneous pattern formation observed in many systems of different kinds in which growth is limited by diffusion, and the question of morphology selection, attract much interest.

The classic models of dendritic growth are continuum models which state the problem in terms of partial differential equations [1,2]. In this picture, the interface is sharp, the diffusion field is smooth, and a Gibbs-Thomson boundary condition is specified on the interface. This leads to a highly nontrivial free boundary problem. Parameters for this approach are macroscopic quantities like surface tension, capillary length, and diffusion constants. These models agree very well with experiments, and continue to furnish interesting results [3]. We want to show in this paper that macroscopic equations can be derived from a microscopic model using the methods of out-of-equilibrium statistical mechanics.

Various microscopic discrete growth models have been investigated. Usually, random walkers are used to approximate the diffusion equation. The most studied model is diffusion-limited aggregation (DLA), invented by Witten and Sander [4]. It would be desirable to obtain the macroscopic description by some kind of continuum limit of the microscopic dynamics. However, the problem of noise is nontrivial in this passage [5]: the approximation of the diffusion equation by random walkers is valid only if a large number of walks are averaged, whereas, in classical DLA, each particle reaching the aggregate sticks immediately. This produces well-known irregular shapes. To model dendrites, one must obtain smooth shapes. Progress in this direction has been made, for example by the introduction of noise-reduced DLA [6], or by models which incorporate curvature effects [7,8]. In all these cases, however, the desired effect is achieved by some algorithmic prescription, which introduces a different parameter (the noise-reduction parameter or sticking probability). There is no precise relation between these parameters and the macroscopic quantities of the continuum approach. Thus we conclude that there is still a ''missing link'' between the microscopic and continuum models.

In this paper we present a model which partially fills in this gap. We start from a stochastic lattice gas with attractive nearest-neighbor interaction, and establish its mean-field kinetic equations by a method recently developed by one of the authors and subsequently applied to the case of an order-disorder transition [9]. The mean-field approximation changes the stochastic process into a system of coupled nonlinear differential equations (dynamical system) without noise. Our model exhibits two-phase coexistence below a critical temperature and a first-order phase transition. Its statics are completely equivalent to those of the usual Ising model, but, in contrast to the widely studied Kawasaki exchange dynamics [10], in our model the dynamics are not invariant under a global spin-flip. We show that our equations of motion are a discrete version of a generalized Model B dynamics in the classification of Hohenberg and Halperin [11], or, in other words, that they constitute a generalized Cahn-Hilliard equation [12] with a mobility coefficient depending on the shape of the local concentration profile.

Our model has some common features with the phase-field models introduced in recent years [13–16]. They work with a diffusion field coupled to a phase field describing the local thermodynamic state via a Ginzburg-Landau order parameter. The interface is extended in space, and the boundary condition is a ''built-in'' feature of the local thermodynamics. In the present study, we consider the isothermal growth of alloy dendrites from a supersaturated solid solution, so that we work with only one field, the concentration. Our equation of motion incorporates diffusion and aggregation naturally which avoids the introduction of an often arbitrary coupling term. In addition, we have the picture of an underlying microscopic process, absent in standard phase-field models. On the other hand, this connection to microscopic dynamics makes our model less flexible: if we want to

*Electronic address: Mathis.Plapp@Polytechnique.fr
†Electronic address: Jean-Francois.Gouyet@Polytechnique.fr

change a macroscopic parameter, we must modify the microscopic interactions.

Lattice gas models are widely used tools to model phase transitions and nonequilibrium phenomena. So it comes as no surprise that our model reproduces many of the characteristic features of first-order phase transitions: after a quench in the unstable region of the phase diagram, we observe phase separation, whereas in the metastable region we have to put in a supercritical nucleus of one phase (denoted by α) in a supersaturated bath of the other phase (denoted by β). This ''germ'' then grows by diffusion of material from the surroundings. It is precisely in this situation that we observe the characteristic Mullins-Sekerka instability [17] and the emergence of nice ''needle crystals.'' From the continuum theory it is known that the factors which control the shape selection of needle crystals are the anisotropy of the surface tension and attachment kinetics which induce a shift in local equilibrium when the interface moves. In our case, these effects are resumed (to linear order) in a boundary condition at the interface of the form

$$\frac{p^\beta - p^\beta_{\rm eq}}{\Delta p} = d(\theta)K + \beta_0(\theta)v. \tag{1}$$

Here p^β is the occupation probability (equivalent to a concentration) immediately ahead of the advancing front, $p^\beta_{\rm eq}$ its bulk equilibrium value, Δp the equilibrium miscibility gap, $d(\theta)$ the orientation-dependent capillary length, K the total curvature ($K=1/R$ in two dimensions), v the interface normal velocity, and $\beta_0(\theta)$ an orientation-dependent kinetic coefficient.

Our goal is to derive the coefficients $d(\theta)$ and $\beta_0(\theta)$ from the microscopic interactions. The Gibbs-Thomson boundary condition can be derived from the statics, and we directly calculate surface tension and capillary length. A key role is played by the interface thickness, which is related to the correlation length, a physically accessible quantity. We find that the anisotropy of surface tension is mainly due to a variation of this length with orientation, a phenomenon which has already been observed in some phase-field models [14].

To derive the kinetic terms, we have to analyze the dynamics of a planar interface. We can determine the kinetic constant numerically. In addition, we find a modification of the flux-velocity boundary condition due to solute trapping, that is a deviation of the concentration of the growing phase from its equilibrium value. This effect is usually not included in the classic formulations of the dendrite problem, probably because for the velocities encountered in dendritic growth it is small. However, for larger velocities, solute trapping is an experimentally well-documented phenomenon, and theoretic treatments by continuum equations [18] and phase-field models [15] are available. To our knowledge this is the first time that all these phenomena are directly derived from a microscopic model in the context of dendritic growth.

It is clear that with an oversimplified model like ours we cannot make a direct comparison with experiments. Given that our model is isothermal, and that there is no latent heat associated with its phase transition, it could be most closely related to alloy dendrites [19], where heat diffusion can often be neglected and the growth is limited by the chemical interdiffusion of the two species. However normally in this case the phase diagram is more complicated than our simple binary mixture. There is only one parameter in our theory, the coupling $\kappa=\varepsilon/kT$ between nearest neighbors. All macroscopic quantities like surface tension, anisotropy, and capillary length are functions of κ. Evidently, to compare our model to real alloys, it would be necessary to include more interactions so as to have the corresponding phase diagram and to reproduce measurable macroscopic quantities like surface tension correctly. But this presents no conceptual difficulties: the lattice gas model is flexible enough to include other interactions. Here we treat a two-dimensional square lattice, but the model can be adapted to three dimensions and other lattice types without too many difficulties.

The remainder of this paper is organized as follows: in Sec. II, we present our model and derive its equation of motion. In Sec. III, we show some numerical simulations. In Sec. IV, we calculate the surface tension, which in Sec. V serves to determine the capillary length. Section VI discusses the anisotropy of the diffusion coefficient, whereas Sec. VII deals with the dynamics of planar interfaces. Section VIII contains a summary and an overview of further perspectives.

II. MODEL

Consider a square lattice of N sites in two dimensions (coordination number $z=4$). Let n_i denote the occupation number of site i: $n_i=1$ if a particle is present, and 0 otherwise. There can be at most one particle at a site. In addition, we assume an attractive nearest-neighbor interaction, which leads to the Hamiltonian

$$H = -\varepsilon \sum_{\langle i,j \rangle} n_i n_j - \mu_0 \sum_{i=1}^{N} n_i, \tag{2}$$

where ε is the interaction energy (attractive: $\varepsilon>0$), μ_0 is an external chemical potential, and the first sum goes over all nearest-neighbor pairs. Clearly, this is completely equivalent to the Ising model. It is also only another form of the Hamiltonian of a binary alloy: if we have two species of atoms (A and B) with nearest-neighbor exchange energies ε_{AA}, ε_{AB}, and ε_{BB}, respectively, it is easy to verify [20] that by putting $\varepsilon=\varepsilon_{AA}+\varepsilon_{BB}-2\varepsilon_{AB}$, and redefining the corresponding chemical potentials, we can recover the Hamiltonian (2). So ''particle'' and ''hole'' can stand as well for ''A'' and ''B'' atoms, and the model can describe processes in alloys as well as the ''condensation'' processes more closely suggested by the lattice gas terminology.

To define the dynamics, we assume that particles can move only via nearest-neighbor hops. In the alloy picture, this corresponds to a simple exchange of atoms. We thus neglect vacancy or interstitial diffusion. We consider our system to be in contact with a heat bath: temperature is constant, and energy is not conserved. Particles can be introduced or taken out only at the boundaries.

We will rapidly recall that the derivation of a kinetic equation for this model that was previously published in more detail by one of the authors [9]. We are interested in equations of motion for the mean occupation number $p_i=\langle n_i \rangle$. The meaning of the average has to be defined, and there are essentially two possibilities. We can think of a tem-

poral average, where we average n_i over a time interval τ which is much larger than the inverse jump frequency, but much smaller than the characteristic time scale of macroscopic evolution (temporal coarse graining). The second possibility is spatial coarse graining in the spirit of real-space renormalization, which leads to the usual coarse-grained free energy functionals. We will adopt the first point of view to keep the meaning of ε as a direct interatomic interaction (spatial renormalization would lead to an effective interaction).

We now want to write a local master equation. The number of particles being a globally and locally conserved quantity, the ''concentration'' p_i obeys a continuity equation

$$\frac{\partial}{\partial t} p_i = -\sum_k j_{ik}, \tag{3}$$

where the sum goes over the nearest neighbors of i, and the current in the link ik is defined by

$$j_{ik} = \langle n_i(1-n_k) w_{ik}(\{n\}) - n_k(1-n_i) w_{ki}(\{n\}) \rangle. \tag{4}$$

The factors $n_i(1-n_k)$ take care of the exclusion principle: the start site must be full, the arrival site empty. $w_{ik}(\{n\})$ are transition probabilities depending on the local configuration. The physical picture behind our model is that the lattice points are located at the equilibrium positions of atoms in a crystal structure. Then an atom is trapped at its site in a potential well whose depth depends on the local configuration. If the thermal energy is small compared to the barrier heights, the jump probabilities follow an Arrhenius law. We assume the barrier height to be the energy necessary to take away an atom from its site, that is, the sum of its binding energies. This leads to

$$w_{ik}(\{n\}) = w_0 \exp\left(\frac{\varepsilon}{kT} \sum_a n_{i+a} \right). \tag{5}$$

w_0 is an isolated particle jump frequency which sets the overall time scale, and will be taken to be unity for convenience. Here and in the following, **a** will denote a lattice unit vector, and summation over **a** means summation over all nearest neighbors. We remark that this expression differs from the usual Monte Carlo rule, where the transition rate is proportional to $\exp(-\Delta H/2kT)$ with ΔH being the energy difference between initial and final states. In our model, the transition rate depends only on the initial state. At this point the asymmetry between particles and holes enters into the dynamics, because an atom surrounded by attractive neighbors will stay in its place much longer than a hole surrounded by other holes.

Finally, we make a mean-field approximation; that is, in all the above expressions we replace the occupation numbers n_i by their mean values p_i. Defining the coupling $\kappa = \varepsilon/kT$ and putting all the pieces together, we have ($w_0 = 1$):

$$\frac{\partial p_i}{\partial t} = -\sum_k \left\{ p_i(1-p_k) \exp\left(-\kappa \sum_a p_{i+a} \right) - p_k(1-p_i) \exp\left(-\kappa \sum_b p_{k+b} \right) \right\}, \tag{6}$$

which constitute the equations of motion (EOM) for our system. Clearly, a mean-field approximation is rather drastic, especially in two dimensions. But, as usual, we hope to obtain a qualitative understanding by this simple treatment. A possible improvement would be to use the path-probability method devised by Sato and Kikuchi [21] or a dynamic density-functional approach [22], but the formulas are considerably more complicated. A study of these issues will be the subject of a forthcoming work.

We can cast these equations in a form more closely connected to out-of-equilibrium thermodynamics. Let us rewrite the expression for the current in the form

$$j_{ik} = -S_{ik}(C_k - C_i), \tag{7}$$

where [we consider the case $s=0$ of Eqs. (10) in Ref. [9]]

$$S_{ik} = \frac{1}{c_0}(1-p_i)(1-p_k) \tag{8}$$

is a term symmetric in the two sites, and

$$C_i = c_0 \frac{p_i}{1-p_i} \exp\left(-\kappa \sum_a p_{i+a} \right) \tag{9}$$

is a local term. This term can be thought of as a local activity,

$$C_i = \exp(\mu_i / kT), \tag{10}$$

and μ_i is a local chemical potential. Then we can rewrite the equation for the current in the form of generalized transport equations:

$$j_{ik} = -M_{ik}(\mu_k - \mu_i), \tag{11a}$$

$$j_{ik} = -D_{ik}(p_k - p_i), \tag{11b}$$

with a generalized mobility

$$M_{ik} = S_{ik} \frac{C_k - C_i}{\mu_k - \mu_i}, \tag{12}$$

and a generalized diffusion coefficient

$$D_{ik} = S_{ik} \frac{C_k - C_i}{p_k - p_i}. \tag{13}$$

Both of these generalized transport coefficients include a dependence on concentration as well as gradient and curvature terms. The connection with well-known field-theoretic models [11] can be established by setting

$$\mu_i = \frac{\partial F(\{p\})}{\partial p_i}, \tag{14}$$

$F(\{p\})$ being a lattice version of a free energy functional. We can choose the arbitrary constants c_0 in Eqs. (8) and (9) and μ_0 in the Hamiltonian (2) in order to make the free energy symmetric and the chemical potential antisymmetric with respect to the interchange $p_i \to 1-p_i$ (particle-hole symmetry). Then we find the following expressions:

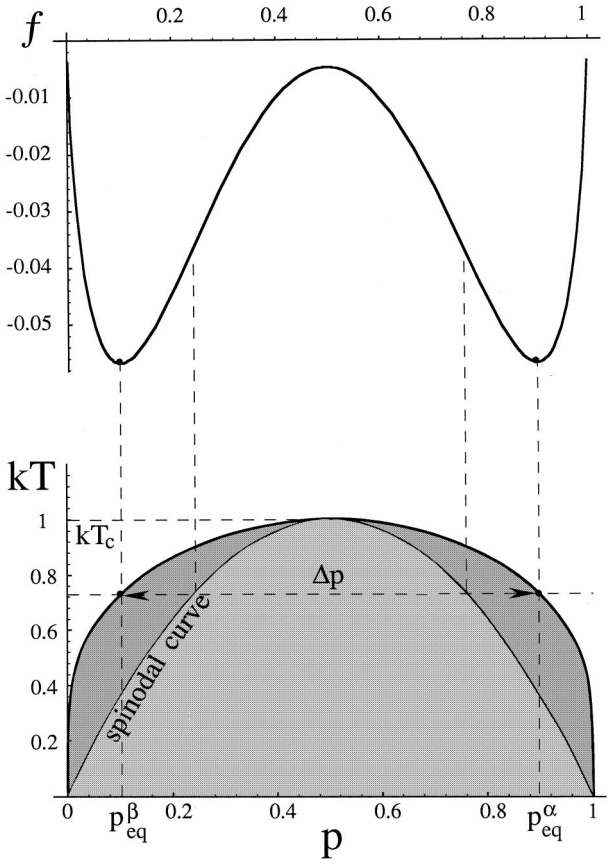

FIG. 1. Local free energy f as a function of p for a temperature $T<T_c$ and the mean-field phase diagram of a simple binary mixture: the two equilibrium concentrations $p^{\alpha}_{\rm eq}$ and $p^{\beta}_{\rm eq}$ correspond to the minima of f. The regions in light grey are unstable; the dark grey corresponds to metastable states.

$$F(\{p\})=\sum_k \left(f_k+\frac{\varepsilon}{4}\sum_a (p_{k+a}-p_k)^2\right), \tag{15}$$

with a local potential

$$f_k=-\frac{z\varepsilon}{2}(p_k-\tfrac{1}{2})^2+kT[p_k\ln p_k+(1-p_k)\ln(1-p_k)]. \tag{16}$$

Here z is the coordination number of the lattice. This is a discrete analog of a continuous functional of the Ginzburg-Landau type, with ε playing the role of a gradient energy,

$$F=\int \left(f(p)+\frac{\varepsilon a^2}{2}(\nabla p)^2\right) dV. \tag{17}$$

Below the critical temperature $kT_c=z\varepsilon/4$, and f_k has a double-well structure with two minima distributed symmetrically around $\frac{1}{2}$. Near kT_c, it can be closely approximated by a quartic potential. For lower temperatures, higher order terms become more important. The two potential wells become very sharp and are located very close to 0 and 1 (Fig. 1).

The chemical potential becomes

$$\mu_k=-\varepsilon\sum_a (p_{k+a}-p_k)-z\varepsilon\left(p_k-\frac{1}{2}\right)+kT\ln\frac{p_k}{1-p_k}. \tag{18}$$

In the first term we recognize a discrete Laplacian: this chemical potential takes into account local curvature of the concentration profile, a natural extension as already noticed by Cahn [23].

We remark that the EOM [Eq. (6)] indeed describe a system approaching equilibrium: when we calculate the total time derivative of the free energy F, we find

$$\frac{dF}{dt}=-\tfrac{1}{2}\sum_{i,k} M_{ik}(\mu_k-\mu_i)^2. \tag{19}$$

M_{ik} always being positive, the free energy can only decrease, and the stationary states satisfy $\mu_k\equiv$const, as expected for equilibrium states.

Now we are ready to establish the (well-known) phase diagram: we are looking for the minima of the free energy, considering only homogeneous states. So $p_k\equiv p$ and the equilibrium concentrations are given by the solutions of the equation

$$\mu(p)=\frac{\partial F(p)}{\partial p}=-z\varepsilon\left(p-\frac{1}{2}\right)+kT\ln\frac{p}{1-p}=0. \tag{20}$$

Below the critical temperature there are two stable solutions, $p^{\alpha}_{\rm eq}$ and $p^{\beta}_{\rm eq}$. Here and in the following, α will denote the dense (''liquid'', ''A rich'') phase and, β the dilute (''gaseous'', ''B rich'') phase. The classical spinodal is given by the solutions of

$$\frac{\partial\mu(p)}{\partial p}=-z\varepsilon+\frac{kT}{p(1-p)}=0, \tag{21}$$

in our case a parabola. The corresponding phase diagram (Fig. 1) is typical of a binary mixture (liquid or alloy): the order parameter is the miscibility gap $\Delta p(T)=p^{\alpha}_{\rm eq}(T)-p^{\beta}_{\rm eq}(T)$. The transition is first order except at the point $p=\frac{1}{2}$, which corresponds to zero magnetic field in the Ising model. Let us remark that this is exactly the mean-field phase diagram of the Ising model. So the statics are completely symmetric with respect to the interchange of particles and holes. But the dynamics are not. If in expressions (12) and (13) for mobility and diffusion constants we take the limit of homogeneous systems, we find

$$M_{\rm hom}(p)=\frac{p(1-p)}{kT}\exp(-\kappa z p) \tag{22}$$

for the mobility and

$$D_{\rm hom}(p)=(1-\kappa z p(1-p))\exp(-\kappa z p) \tag{23}$$

for the diffusion coefficient. We see that the exponential term destroys the symmetry: dynamics is slower in the dense phase. The temperature can be used to ''tune'' the ratio between the diffusion constants in the two bulk phases: we have, in view of the symmetry of the two equilibrium concentrations,

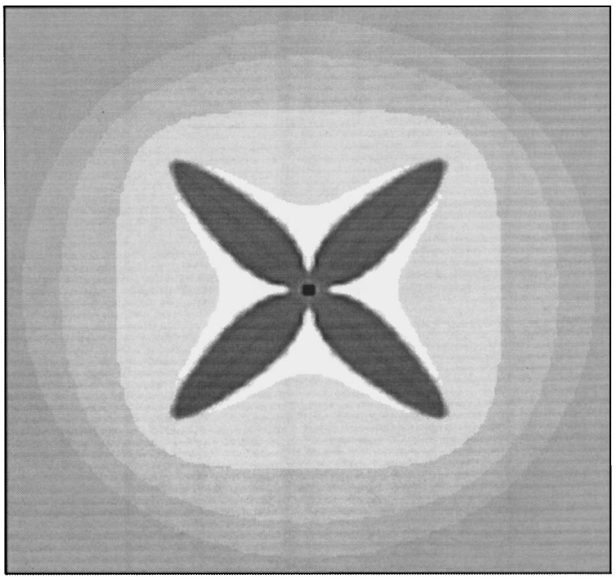

FIG. 2. Fourfold ''snowflake'' grown on a 200×200 square lattice at $T=0.1T_c$, and a fixed concentration on a large circle $p_\infty=0.02$.

$$\frac{D_{\rm hom}(p_{\rm eq}^{\alpha})}{D_{\rm hom}(p_{\rm eq}^{\beta})}=\exp(-\kappa z\Delta p), \tag{24}$$

where the miscibility gap Δp is a function of temperature. The widely used symmetric model, where this ratio is taken to unity, is approached only in the limit $T\to T_c$.

III. SIMULATIONS

We studied the behavior of our model by numerical simulations. To this end, we must integrate the equations of motion. We used a simple Euler finite difference algorithm. As usual in such algorithms, the speed of the calculation is limited by a numerical instability which occurs when the timestep becomes too large. The limit on the timestep can be calculated by a linear stability analysis. We performed simulations with timesteps near this limit, and control runs with smaller timesteps gave the same results. All simulations presented in this section are performed on a standard workstation, and each took several hours CPU time. The biggest lattices we used are 200×200 points.

To observe diffusion-limited growth, we chose as initial condition some ''seed'' of the α phase surrounded by a ''bath'' of supersaturated β phase: the concentration p_∞ at the exterior of the droplet must be bigger than $p_{\rm eq}^{\beta}$ to have a nonzero thermodynamic driving force, and smaller than the concentration on the spinodal to avoid nucleation. In this situation a concentration gradient develops and drives a diffusive flux toward the interface. It is easy to see that for small gradients the EOM (6) reduce to a diffusion equation. For low temperatures, we observe the formation of four-spoked snowflakes as depicted in Fig. 2. To speed up growth, we held the concentration constant and equal to p_∞ at the exterior of a circle. We emphasize that this does *not* correspond to free dendritic growth in supersaturated solutions, but for the moment we are interested only in the qualitative features of the branching instability, and not in the detailed

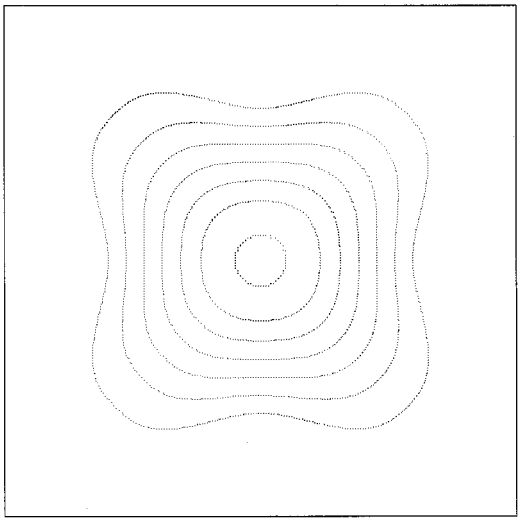

FIG. 3. Stroboscopic plot of a growing droplet on a 200×200 lattice, starting from a circular initial state (radius $R=10$), showing the Mullins-Sekerka instability. $T=0.5\ T_c$ and $p_\infty=0.1$.

finger shapes. We checked that the overall shape of the aggregate is independent of the boundary conditions. To observe the initial stages of the branch formation in greater detail, in Fig. 3 we show a stroboscopic plot of a growing circular germ at higher temperature. The aggregate develops small bulges in the diagonals of the lattice which grow gradually to form fully developed branches. This is the well-known Mullins-Sekerka instability [17].

What interests us here is the mechanism which favors growth in the lattice diagonals, and stabilizes the tip of the growing needles. From macroscopic theories it is known that a necessary prerequisite for the existence of stable growing tips is an anisotropy of the surface tension. This effect exists in our model, but there might be other effects due to the lattice: the diffusion coefficient, which ''lives'' on the lattice bonds, might be anisotropic, and the attachment kinetics could play an important role. To solve this puzzle, we will treat each of those effects separately in the following sections. We remark that the favored growth directions are stable: when we start growth with an initial condition presenting tips in the lattice directions, these tips become unstable and split to form two new tips in the diagonals. This is depicted in Fig. 4.

The simulations of Figs. 2 and 3 have the same lattice size. Hence we see that there is a global scaling with temperature. This is due to the fact that the intrinsic length scale of our model is the characteristic interface width ξ, which is shown below to diverge when T approaches T_c. However, given the dependence of the dynamics on temperature as expressed in Eq. (24), we expect this not to be a simple renormalization of lengths.

It is clear that for a temperature of $T=0.1\ T_c$ as in Fig. 2, this characteristic length is much smaller than the lattice constant, which means that the mean-field approximation is the least doubtful. Our analytical developments presented below are strictly valid only at high temperatures ($T\geqslant 0.7T_c$). However, our numerical results indicate that there is no qualitative change. To have simulations corresponding to well con-

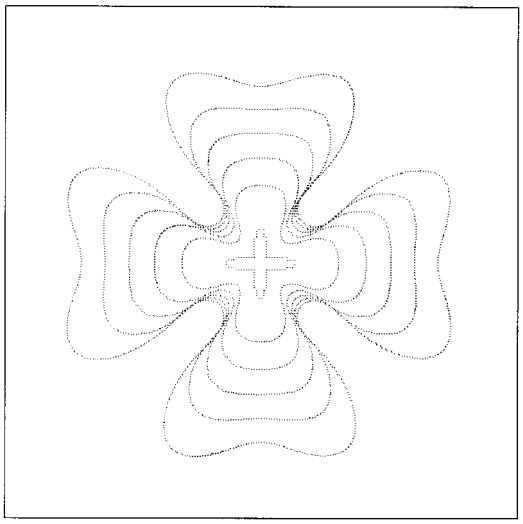

FIG. 4. Same as Fig. 3, but starting from a seed presenting tips in the lattice directions, which are unstable growth directions.

FIG. 5. Same as Fig. 2, but a conservative Langevin noise term is added to the equations of motion: sidebranches appear.

trolled analytics, we would have to increase the system size and temperature, which means larger CPU times. This is currently being done.

Another important issue is noise. Real dendrites are not needle crystals, but present sidebranches. To observe sidebranching in our model, we have to add noise. We can do this either by adding a conservative noise term to the equations of motion or by adding a quenched noise: at each site, we assign a randomly chosen local energy. In both cases, sidebranches develop. Figure 5 shows a picture generated with the former method. The fact that sidebranching activity is connected to noise is known, but a quantitative description is still lacking.

Even for the deterministic evolution, a noisy initial condition may lead to chaotic behavior when the average concentration gradient is not parallel to one of the growth directions. Figure 6 shows a simulation in cylindrical geometry (periodic boundary conditions in the y direction), where we placed a ''substrate'' at the bottom which consists of one layer of solid and one layer of ''rough'' surface, where the concentrations were chosen at random between 0 and 1. At the top, the concentration was fixed. We see that the initial noise is sufficient to destabilize the planar surface: dendrites with sidebranches occur.

The characteristic width of the developing structures depends both on temperature and incoming flux. It is known from dendritic growth theory that the tip radius R of the selected dendrites is roughly the geometric mean of the capillary length d_0 and the diffusion length D/v, where v is the tip velocity:

$$R \approx \sqrt{d_0 D/v}. \tag{25}$$

Given that the former is proportional to the correlation length ξ, whereas the latter is inversely proportional to the velocity, the structures should sharpen when the temperature goes down or the flux goes up, which is indeed what we observe.

We will now analyze more in detail the different factors contributing to the anisotropy, and if possible give analytic expressions for the various effects. These will be checked against numerical calculations.

IV. SURFACE TENSION

It should be clear from the beginning that all effects of anisotropy are due to the lattice, and hence invisible in a continuum treatment of the problem. For the sake of comparison, let us nevertheless recall very briefly the continuum definitions.

Consider a planar interface whose normal coordinate is x. At equilibrium, the chemical potential is constant throughout the system, and for planar interfaces it is zero by symmetry. If the concentration varies slowly on the scale of the lattice spacing a, Eq. (18) can be approximated by

$$-\varepsilon a^2 \frac{\partial^2 p(x)}{\partial x^2} + f'(p(x)) \equiv 0. \tag{26}$$

Multiplying both sides with dp/dx and integrating once gives

$$\tfrac{1}{2}\varepsilon a^2 \left(\frac{\partial p}{\partial x}\right)^2 = f(p) - f(p_{\mathrm{eq}}), \tag{27}$$

a relation which, in the language of the well-known mechanical analog, expresses the equipartition of kinetic and potential energies. The surface tension is defined as the excess free energy per unit surface,

$$\sigma = \frac{F_{\mathrm{int}} - F_{\mathrm{hom}}}{S}, \tag{28}$$

where F_{int} and F_{hom} are the free energies of the equilibrium states with and without an interface, respectively. Using the free energy functional (17) and the relation (27), we have, in two dimensions,

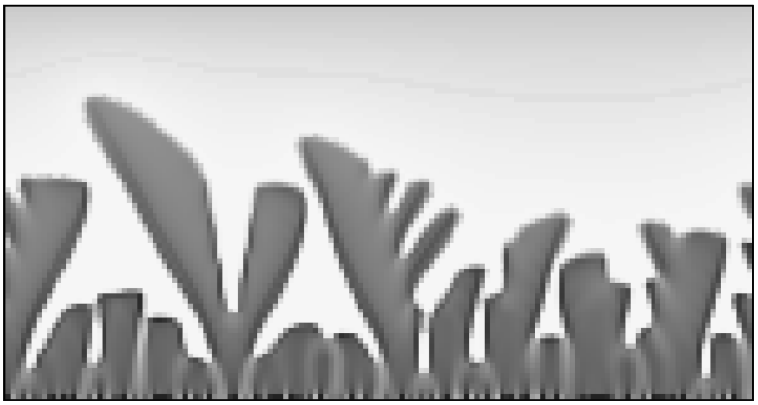

FIG. 6. Growth from a rough interface on a 150×80 lattice. Concentration in the second ''substrate'' layer varies randomly between 0 and 1; no other noise is added. The concentration far from the substrate is fixed to 0.02, and $T=0.1T_c$.

$$\sigma=\varepsilon\int_{-\infty}^{\infty}\left(\frac{\partial p_0(x)}{\partial x}\right)^2 dx, \tag{29}$$

where $p_0(x)$ is the solution of the differential equation (26) subject to the appropriate boundary conditions; that is, the solution which connects the two equilibrium concentrations.

For a quartic potential, the exact solution $p_0(x)$ is a hyperbolic tangent; for nearly all double-well potentials, the tanh is a good approximation. (Small) corrections can be easily calculated (see below). We can determine the characteristic thickness ξ of the interface by a well-known method (see, for example, Ref. [24]). Far from the interface, the concentration approaches the equilibrium value $p_{\rm eq}$ (in view of the symmetry of the two phases, here we will drop the superscripts α and β). Writing $u(x)=p(x)-p_{\rm eq}$ and linearizing (26) in u yields

$$-\varepsilon a^2 u''(x)+\mu'(p_{\rm eq})u(x)=0. \tag{30}$$

The solution is an exponential, $u\approx\exp(x/\xi_0)$, where the interface width is given by

$$\xi_0=a\sqrt{\varepsilon\chi_{\rm eq}}. \tag{31}$$

Here, we have defined the susceptibility $\chi(p)$ by

$$\chi(p)^{-1}=\frac{\partial\mu(p)}{\partial p}, \tag{32}$$

and $\chi_{\rm eq}=\chi(p_{\rm eq})$. This characteristic length depends on temperature and diverges with power $\frac{1}{2}$ as T approaches the critical temperature, as expected for a mean-field correlation length.

Let us, then, approximate the equilibrium interface to zeroth order by

$$p_0(x)=\tfrac{1}{2}+\frac{\Delta p}{2}\tanh\left(\frac{x}{2\xi_0}\right) \tag{33}$$

(Δp is the miscibility gap). Calculating integral (29), the continuous surface tension is given by

$$\sigma_c=\frac{\varepsilon(\Delta p)^2}{6\xi_0}. \tag{34}$$

Now we are ready to make comparisons to our discrete system. The exact equilibrium states can be found numerically by solving the set of equations $\mu_k=0$, subject to the appropriate boundary conditions which enforce an interface in a given direction. For the symmetry directions (10) and (11) this is fairly simple, because the problem reduces to an array of equations for points on a line, which can be indexed by an integer. Therefore, we can use Eq. (18) for an iterative solution. To do this, we can start out, for example, at the symmetric point $p_0=\frac{1}{2}$. Then we have to pick p_1 and iterate Eq. (18). p_1 has to be chosen in order to satisfy the boundary condition $p_k\to p_{\rm eq}$ for $k\to\infty$. By a simple ''shoot and test'' algorithm we can obtain great precision very rapidly. Equation (18) is the discrete analog of a differential equation, so it is not surprising that only the boundary condition can select a solution. Another quite rapid method to obtain exact interface shapes is simply to use the equations of motion and let the system relax to the equilibrium state.

Once the equilibrium state is known, we can use the basic definition (28) and our discrete free energy functional (15) to determine the surface tension. We find that for the square lattice at all temperatures the surface tension in the lattice diagonals, σ_{11}, is slightly higher than along the lattice axes, σ_{10}. In addition, the surface tension depends on the position of the interface with respect to the lattice. If we define the position of the interface by the symmetric point $p=\frac{1}{2}$, σ is extremal when the interface is exactly on a lattice point (''odd number of sites'') and in the middle between two points (''even number of sites''). This is a consequence of the discrete structure of our model. It is known that in some situations as e.g., in epitaxial growth, physical quantities vary with the coverage, that is, with the average occupation number of a given crystal plane. However, it seems difficult to establish a direct relation to such phenomena by our mean-field treatment. We remark, however, that our model leads to physically reasonable behavior. First, these variations are much weaker in the (11) direction than in the (10) direction. Arguing in terms of the stochastic process, this can be understood from the fact that an atom arriving on a (11) surface has two connected links, independent of the coverage, whereas on a (10) surface this number varies between 1 (nearly empty surface) and 3 (nearly filled surface). Second, consider a vicinal surface, that is, an interface making a

small angle with a singular direction. The interface will tend to attach to its configuration of lowest surface tension, which will cause the formation of well-localized steps if the interface is not too thick. This is the case in our model for temperatures below $T \approx 0.7 T_c$. For higher temperatures, the effect decays rapidly: for $T = 0.8 T_c$, the amplitude of the variations of σ with position is only about 1% of the amplitude of angular variations, and it decays much more rapidly when we approach the critical temperature. This allows us to neglect it in the high-temperature domain, corresponding to rough interfaces.

We make the approximation that the profile of the interface is invariant under translation parallel to the surface; that is, the concentration at a given lattice point depends only on the projection of its coordinate vector onto the normal. Consider a planar interface whose normal **n** makes an angle θ with a lattice axis. We will denote by x the projection of the coordinate on **n**. A first consequence of the lattice structure is that the thickness ξ becomes dependent on θ. This can be seen as follows. Instead of Eq. (26), we now have to linearize the discrete equation (18). Writing $p_k = p_{\mathrm{eq}} + u_k$, and explicitiing the discrete Laplacian, we find.

$$-\varepsilon\big(u(x + a\,\cos\theta) + u(x - a\,\cos\theta) + u(x + a\,\sin\theta) + u(x - a\,\sin\theta) - 4u(x)\big) + \mu'(p_{\mathrm{eq}})u(x) = 0. \quad (35)$$

We see that this equation is solved by $u(x) = \exp(x/\xi(\theta))$, provided that

$$\cosh\left(\frac{a\,\sin\theta}{\xi(\theta)}\right) + \cosh\left(\frac{a\,\cos\theta}{\xi(\theta)}\right) - 2 = \frac{1}{2\varepsilon\chi_{\mathrm{eq}}}. \quad (36)$$

From this equation, we can determine $\xi(\theta)$. For high temperatures where ξ is not too small, we can expand in ξ and obtain, to leading order in θ,

$$\xi(\theta) = \xi_0\left(1 + \frac{1}{32\varepsilon\chi_{\mathrm{eq}}} + \frac{1}{96\varepsilon\chi_{\mathrm{eq}}}\cos 4\theta\right), \quad (37)$$

where ξ_0 is given by Eq. (31). There is a general correction to the continuum result due to the finite lattice step, plus an explicit anisotropy, which displays the fourfold symmetry of the square lattice. As expected, for $T \to T_c$, the details of the lattice structure are suppressed (the susceptibility diverges): we recover the continuum result, and the anisotropy vanishes.

If we use this result together with the ansatz (33) and the continuum formula (34) to calculate a first order approximation to the surface tension, we find

$$\sigma(\theta) = \sigma_c\left(1 - \frac{1}{32\varepsilon\chi_{\mathrm{eq}}} - \frac{1}{96\varepsilon\chi_{\mathrm{eq}}}\cos 4\theta\right). \quad (38)$$

Comparing this result to the exact values for $\theta = 0$ and $\theta = \pi/4$, we find that the values of σ are well reproduced for high temperatures. On the contrary, the anisotropy $(\sigma_{10} - \sigma_{11})/(\sigma_{10} + \sigma_{11})$ is largely overestimated even for high temperatures (Fig. 7). The reason is that the anisotropy contains the difference of two surface tensions, which is a second order term and needs more precise calculations. The

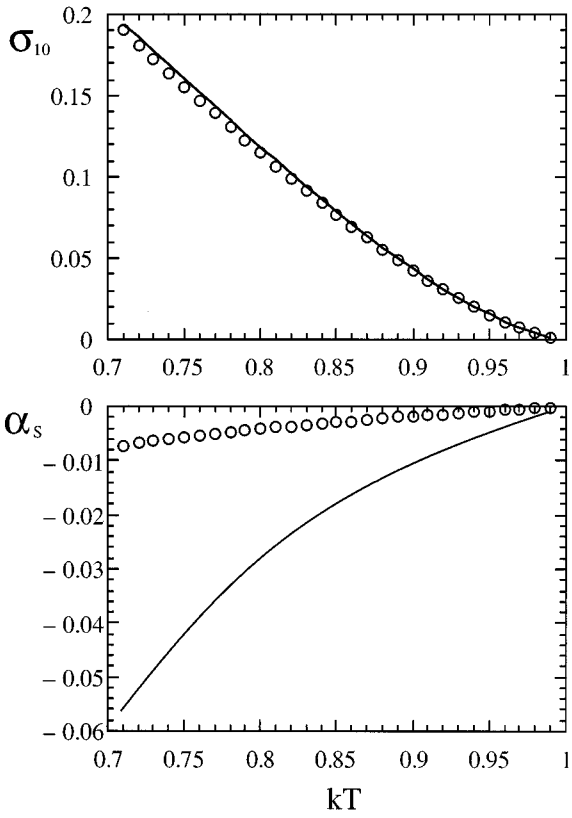

FIG. 7. Surface tension in the lattice directions and anisotropy as a function of temperature. Circles are numerical results, lines the the first-order approximation (38). Using the improved method (40), we obtain a perfect agreement.

anisotropy is an important control parameter in the dendrite problem, and hence we will make some effort to obtain better results.

There are two reasons for the difference between Eq. (38) and the numerical results. The first is the use of the continuum relation (29). The passage from Eqs. (26) to (27) makes use of the chain rule, which is valid for the continuum case but not for finite differences. This means in particular that the equipartition of the energy is no longer valid. Indeed, if we try to improve our result by using simply the discretization of Eq. (29), we find that the anisotropy changes sign. So there is an important contribution from the potential energy, and we have to use the complete definition (28) to evaluate σ.

The second reason is the use of the ansatz (33). It is a good approximation of the equilibrium solution far from the interface, but not around the origin, which makes the most important contribution to the surface tension. When we compare the exact profiles with Eq. (33) using the appropriate discrete $\xi(\theta)$, we indeed find that the differences are localized around the origin. Moreover, we find that in the (10) direction the interface is steeper than predicted by (33), whereas in the (11) direction it is flatter.

To account for the second effect, we must improve our ansatz by adding a correction $g(x)$. This correction should be antisymmetric, and decay to 0 faster than $\exp(x/\xi)$ in order to leave the limit values and the linear order terms as fixed by Eq. (35). If we expand the potential in Eq. (18) in powers of $(p - \frac{1}{2})$, we see that powers of the initial tanh function can be

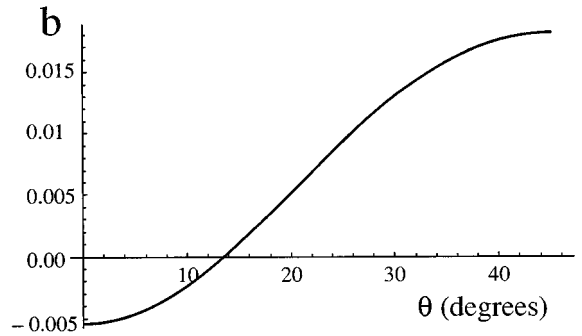

FIG. 8. Plot of the coefficient $b(\theta)$ of the shape correction to the hyperbolic tangent profile given by Eq. (39), for $T=0.86T_c$.

candidates for an improved solution, for then we can solve order by order. To satisfy the other conditions on $g(x)$, we choose $g(x)=bd^2/dx^2\tanh(x/2\xi)$, which leads to the following ansatz:

$$p(x)=p_0(x)+g(x)=\frac{1}{2}+\left(\frac{\Delta p}{2}-\frac{b}{2\xi^2}\right)\tanh\left(\frac{x}{2\xi}\right)+\frac{b}{2\xi^2}\tanh^3\left(\frac{x}{2\xi}\right). \tag{39}$$

Hereby, we introduce another degree of freedom, the parameter $b(\theta)$, which has to be fixed. To achieve this, we use the complete equation (18), taken at a point x_0 not far from the origin, which we solve numerically for b. The result depends on the choice of x_0: here we recover the variation of the surface tension with the interface position. As discussed above, for high temperatures this effect is negligible. An example of a plot of $b(\theta)$ is shown in Fig. 8. We see that b changes sign between the symmetry directions, giving good agreement with the numerical calculations.

Then we can calculate $\sigma(\theta)$ using the discrete formulas (15) and (28). The results in the high-temperature region are very good: they agree up to the fifth decimal with the numerics. This method is easy to handle, because it needs only the numerical solution of one equation instead of the optimization procedure necessary to obtain the exact interface shape.

Figure 9 shows a plot of $\sigma(\theta)$. We see that it can be very well approximated by a fit of the form

$$\sigma(\theta)=\sigma_0(1+\alpha_S\cos 4\theta), \tag{40}$$

where $\sigma_0=(\sigma_{10}+\sigma_{11})/2$, and the anisotropy of the surface tension is

$$\alpha_S=\frac{\sigma_{10}-\sigma_{11}}{\sigma_{10}+\sigma_{11}}. \tag{41}$$

In fact, when we subtract a cosine from the numerical results, we see the next harmonic, $\cos(8\theta)$, with a very weak amplitude. So the functional form given by the leading order analysis is correct, and, when high numerical precision is necessary, we can work with Eq. (40) instead of Eq. (38). For the square lattice the surface tension has maximum values in the diagonals, which gives a negative anisotropy with definition (41). This corresponds to the usual conventions. We can easily repeat similar calculations for other lattice types, e.g., the triangular lattice ($z=6$). Here we find a weaker sixfold anisotropy, this time with the maxima of the surface tension in the lattice directions. Simulations analogous to Fig. 2 indeed show six-spoked snowflakes with their arms pointing in the lattice directions.

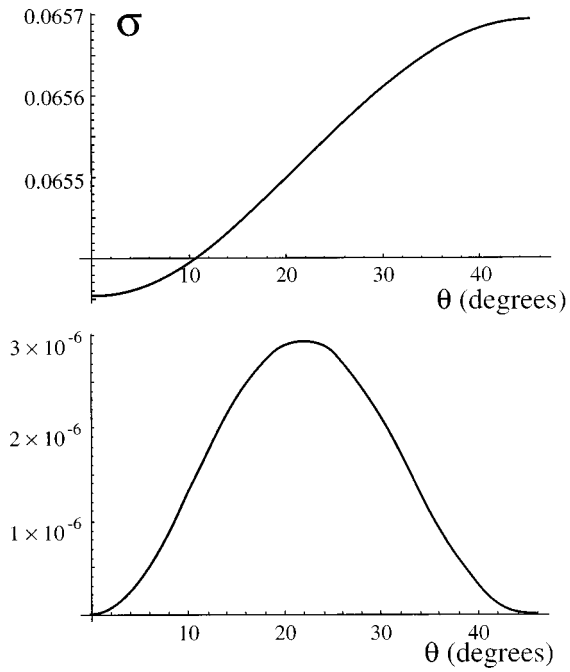

FIG. 9. Surface tension as a function of orientation for $T=0.86T_c$. Below: difference of the upper curve and the pure cosine given by Eq. (40): the next harmonic, $\cos(8\theta)$, appears.

V. GIBBS-THOMSON BOUNDARY CONDITION AND CAPILLARY LENGTH

Curved interfaces modify the local equilibrium concentrations. Contrary to the planar case, there is symmetry breaking between droplet and exterior, which leads to a nonzero chemical potential. When the radii of the curvature are much larger than the lattice constant, we can use a continuum approximation. For isotropic surface tension, it is straightforward to show [24] that the first order correction to concentrations in and out of a droplet is

$$p-p_{\rm eq}=\Delta p\left(1+\frac{a^2\sigma\chi_{\rm eq}}{(\Delta p)^2}K\right), \tag{42}$$

where K is the local curvature of the interface, counted positive for a droplet of ''liquid'' in a bath of ''vapor.'' The fact that its value is the same in both phases is due to the equality $\chi(p^{\alpha}_{\rm eq})=\chi(p^{\beta}_{\rm eq})=\chi_{\rm eq}$ in our model. The coefficient of K defines the capillary length. From Eq. (20), Eqs. (30) and (34) we can see that it is proportional to ξ. This could have been expected because in the continuum limit ξ is the only intrinsic length scale. Herring showed [25] that, for an anisotropic surface tension, this condition has to be modified; the capillary length d becomes a function of orientation, and the surface tension is replaced by the interface stiffness

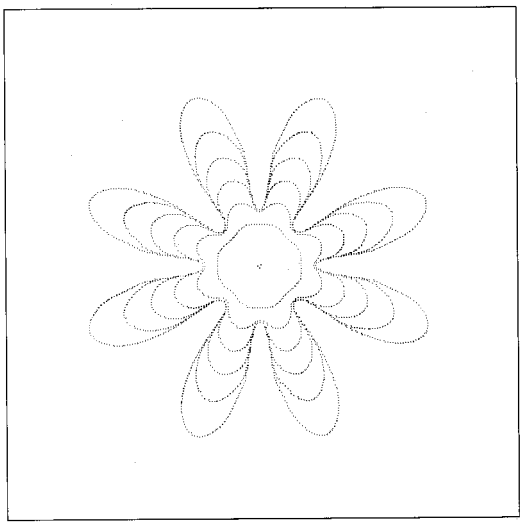

FIG. 10. Same as Fig. 2, but a next-nearest-neighbor interaction has been introduced. For $T=0.1T_c$, $p_\infty=0.02$, and $\varepsilon_1/\varepsilon_2=2$, we obtain eightfold structures.

$$d(\theta)=\frac{a^2\chi_{\rm eq}}{(\Delta p)^2}\,(\sigma(\theta)+\sigma''(\theta)), \tag{43}$$

where σ'' denotes the second derivative of σ with respect to θ. Using expression (40), we find that

$$d(\theta)=\frac{a^2\chi_{\rm eq}\sigma_0}{(\Delta p)^2}\,(1-15\alpha_5\cos 4\theta). \tag{44}$$

The capillary length stays roughly proportional to the correlation length, and diverges at the critical temperature. The anisotropy is a function of temperature only, and vanishes at the transition, where all details of the lattice structure are wiped out. In real systems, the capillary length is usually of the order of nanometers, that is, at least one order of magnitude above the interatomic spacing. In our model we reach this order of magnitude only for $kT_c-kT<10^{-2}$. In the simulations presented in Sec. III the capillary length is smaller than the lattice constant. This is not in contradiction with the continuum approach, because the physical quantity is the product (dK), which gives the concentration deviation at the interface. As long as the tip radius given by Eq. (25) stays reasonably larger than the lattice constant, this approach should be valid.

We see that we cannot vary capillary length and anisotropy independently. To do this, we would have to introduce another free parameter (besides the temperature). The natural choice is to introduce more interactions. For example, by introducing next-nearest-neighbor interaction and playing with the ratio between the two interaction strengths, we succeeded in screening the fourfold component of the anisotropy completely, arriving at eightfold structures (Fig. 10). Increasing the range of the interaction, we thus can alternatively approach isotropic growth or achieve a desired anisotropy.

We can compare our result to the standard boundary condition used in two dimensions. We see that the favored growth directions, which are marked by a minimum of the capillary length, are indeed the diagonals. Hence we have shown that the Gibbs-Thomson effect can explain the formation of stable dendrite tips in the lattice diagonals. We now have to analyze the other possible effects.

VI. ANISOTROPY OF THE DIFFUSION COEFFICIENT

In the region surrounding the growing aggregate, the concentration gradients are small. The equation of motion reduces to a diffusion equation. However, the currents and concentrations are defined on the lattice, and expression (13) for the diffusion coefficient involves discrete Laplacians via the chemical potentials. Hence the diffusion coefficient varies as a function of the orientation of the concentration gradient. Starting out from an initial condition with rotational symmetry as in Fig. 3, this leads to a variation of the currents with the orientation which could cause the formation of tips where the diffusion is enhanced. We will now analyze this anisotropy.

Imagine a uniform concentration gradient $\nabla p=(\nabla p_x,\nabla p_y)$ in a certain region of the lattice. We will denote its direction by $\mathbf{n}=(n_x,n_y)$. Then the concentration differences between neighboring sites are $a\nabla p_x$ in the x direction, and $a\nabla p_y$ in the y direction. We choose a reference point of concentration p_0 and develop Eq. (13) to first order in ∇p. The result is

$$D_x=D_{\rm hom}(p_0)(1+\alpha_D(p_0,kT)a\nabla p_x) \tag{45}$$

for a link in the x direction, and the analog for the y direction. $D_{\rm hom}$ is the homogeneous diffusion coefficient defined in Eq. (23), and α_D is given by

$$\alpha_D(p_0,kT)=\frac{1-kT\chi'(p_0)}{2kT\chi(p_0)}-\frac{1}{1-p_0}, \tag{46}$$

χ' denoting the derivative of χ with respect to p. The microscopic currents are $j_x=-aD_x\nabla p_x$ and $j_y=-aD_y\nabla p_y$. The macroscopic current crossing a surface normal to the gradient is then given by the sum over the microscopic currents in all the links that cross the surface. A surface of length L $(L\gg a)$ normal to $\mathbf{n}$ cuts approximately Ln_x links in the x direction, and Ln_y links in the y direction. The resulting macroscopic current (per unit surface) is

$$|j|=a|\nabla p|(D_xn_x^2+D_yn_y^2). \tag{47}$$

Inserting Eq. (45) gives (using the fact that n is a unit vector)

$$|j|=a|\nabla p|D_{\rm hom}[1+a|\nabla p|\alpha_D(|n_x^3|+|n_y^3|)]. \tag{48}$$

We see that the second order introduces anisotropy. The term in n^3 has a maximum value 1 on the lattice directions, and a minimal value $1/\sqrt{2}$ on the diagonals. This anisotropy is proportional to the concentration gradient and to the function α_D. Typical values of $a|\nabla p|$ in our simulations are around 10^{-4}. For high temperature, α_D is negative and of order unity, which makes this anisotropy two orders of magnitude less than the anisotropy of the surface tension. For lower temperatures, α_D begins to grow and becomes positive: in the concentration ranges we used, it is of order 10 for $kT=0.5$, and of order 100 for $kT=0.1$. Still, the resulting anisotropy is small compared to the static anisotropy. Moreover, because α_D is positive, the diffusion coefficient is

slightly higher in the (10) direction. This means that diffusion is enhanced along the lattice directions, which should lead to tips in the lattice directions instead of the observed tips. We conclude that the anisotropy of the diffusion coefficient is not the cause of the observed tip formation.

VII. DYNAMICS OF PLANAR INTERFACES

The first step toward understanding the dynamical behavior of the full model has to be a study of planar interfaces. The curvature is zero, which allows us to isolate kinetic effects. In addition, when the interface is oriented normal to the (10)- and (11)-symmetry directions, we can reduce our array of equations (6) to a quasi-one-dimensional set of equations, which are much easier to handle, analytically and numerically. Then each concentration p_k represents a whole layer of lattice sites. For the (10) direction the reduced version of (6) reads

$$\frac{dp_k}{dt} = w_0 \sum_j \{p_k(1-p_j)\exp[\kappa(p_{k-1}+2p_k+p_{k+1})] - p_j(1-p_k)\exp[\kappa(p_{j-1}+2p_j+p_{j+1})]\}. \quad (49a)$$

whereas for the (11) direction it is

$$\frac{dp_k}{dt} = w_0 \sum_j \{2p_k(1-p_j)\exp[2\kappa(p_{k-1}+p_{k+1})] - 2p_j(1-p_k)\exp[2\kappa(p_{j-1}+p_{j+1})]\}. \quad (49b)$$

The factors 2 in the second formula come from the lattice geometry. In both cases, j takes the values $k-1$ and $k+1$ in the sum. Attention has to be paid to the fact that the points are not at equal spacing: in direction (10), the distance of two layers is a, whereas in direction (11) it is $a/\sqrt{2}$.

These systems of equations can be integrated much more rapidly, and we have carried out extensive numerical studies. We are interested in the departure of the interface shape from the equilibrium shape. This departure depends on the interface velocity v, which in turn is a function of the thermodynamic driving force. To have a time-independent solution, we thus must seek the stationary states; that is, the situations in which v is constant. For a conserved one-dimensional system a traveling front with constant velocity and vanishing concentration gradients at infinity is impossible, because this would violate mass conservation. To have an advancing front, we have to feed a current into the system. After a transient, the profile settles down to a stationary state; that is, the profile $p(x,t)$ should become a function of the reduced variable $u=x-vt$ only. We want to determine the form of this stationary profile as a function of the velocity v, and the relation between current and velocity.

A complete treatment of this issue is beyond the scope of this paper, and will be published elsewhere [26]. We can completely solve a continuum approximation following ideas similar to those of Langer and Sekerka [27], who worked on the continuous Cahn-Hilliard equation. The discrete problem is much more intricate. In fact, given that we have no continuous translational symmetry, a true stationary state might even not exist at all. Indeed, monitoring the dynamics (49) closely, we see that the interface shape and the growth velocity oscillate slightly while the interface advances, with a period that corresponds exactly to one lattice step. This is correlated to variations of the surface tension with the interface position discussed in Sec. IV: the interface slows down when it must ''climb'' a hill of surface tension, and accelerates when it ''slides down'' in the next valley. To investigate the dynamical anisotropy of our system, we have to treat the discrete problem. We will proceed by averaging over one period, which is certainly a valid procedure at high temperatures as discussed above.

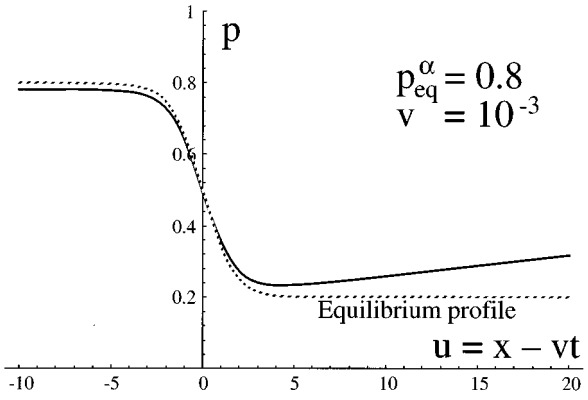

FIG. 11. Stationary interface shape for $T=0.86T_c$ and $v=10^{-3}$, obtained from the continuum treatment to be published [26]. For comparison, the equilibrium profile is displayed as a broken line.

We integrated the sets of equations (49) for various system sizes L, temperatures, and currents. The initial conditions were the corresponding equilibrium shapes centered at a position n_0. As boundary conditions, we imposed zero current at $n=0$ and a current j_0 at $n=L-1$. To calculate the current from site 0 to site 1, we chose ''mirror'' boundary conditions, $p_{-1}=p_0$. To have a stationary state, we used a moving frame: once the interface moved forward by one lattice step, the whole configuration was shifted backward. We found that after a certain transient, the system settled down to a configuration independent of initial conditions. The profiles obtained in this way have the shape depicted in Fig. 11. Behind the moving front, a plateau at concentration p^{α}_{∞} develops. p^{α}_{∞} is a function of the velocity and always smaller than the equilibrium concentration of the dense phase p^{α}_{eq}. The interfacial region preserves the overall shape of the equilibrium profile when the velocity is not too large. Far in front of the interface (at several times the interface thickness ξ), we find a ramp profile where the concentration gradient is nearly constant. The exact solution of the diffusion equation (with D constant) in a moving frame is an exponential; however, in our case the diffusion length $l=D/v$ is of order 10^5, so that we can safely approximate the profile by a straight line. We observe that its intercept p^{β}_0 at the interface position n_0 is also a function of v, and always larger than the equilibrium concentration of the dilute phase, p^{β}_{eq}. For small velocities and high temperatures, p^{α}_{∞} and p^{β}_0 are linear func-

tions of the velocity. At low temperatures, $p_\infty^\alpha(v)$ develops important nonlinearities due to the slow dynamics in the α phase.

How do these modifications influence the macroscopic boundary conditions at the interface? The concentration given by condition (1) is in fact a concentration in the dilute phase immediately ahead of the interface. In our model, this is precisely the value p_0^β defined above. Hence when p_0^β is linear in v, this defines the kinetic coefficient β_0,

$$p_0^\beta - p_{\rm eq}^\beta = v\,\Delta p\,\beta_0 . \tag{50}$$

Plotting the intercept against the velocity, we can determine β_0.

The concentration deviation in the growing phase is known as ''solute trapping.'' It is so called because a certain species of atoms (in our model: the holes) are trapped in the advancing front, even if this increases their chemical potential. This does not influence the boundary condition (1), but it modifies the relation between incoming flux and velocity. To order zero, this relation is given by

$$|j| = v\,\Delta p, \tag{51}$$

where j is the current arriving at the interface. However, this supposes that the current has to ''fill in'' the complete miscibility gap. At nonzero velocity, we have to replace Δp by $p_\infty^\alpha - p_0^\beta$. In the linear region, we write $p_\infty^\alpha - p_{\rm eq}^\alpha = v\,\delta p_\infty^\alpha$. The first correction to Eq. (51) thus reads

$$|j| = v(p_\infty^\alpha - p_0^\beta) \cong v\,\Delta p + v^2(\delta p_\infty^\alpha - \beta_0). \tag{52}$$

We see that the two coefficients δp_∞^α and β_0 are sufficient to determine the coupling of the interface to the diffusion field and the flux-velocity relation (52) in the high-temperature region. We have determined δp_∞^α and β_0 numerically for several temperatures in the two main symmetry directions. The former is negative of order -10 and has a slight anisotropy, which is about 1% for $kT=0.8$, and decays with growing temperature. The latter is of order unity and develops a stronger anisotropy (about 30%) for temperatures between $0.5T_c$ and $0.8T_c$. The higher value is in the (10) direction, slowing down growth in this direction. However, the important difference $\delta p_\infty^\alpha - \beta_0$ shows only a slight anisotropy because the anisotropies of the two coefficients compensate each other. More details will be published soon [26].

We are now ready to make a comparison between kinetic and curvature effects. We have not yet made simulations in two dimensions at sufficiently high temperatures to reach the temperature range in which the analytic developments are valid with certainty. However, our numerical results for one-dimensional systems indicate that there are no qualitative changes when we go to lower temperatures. We will therefore compare with the data from our simulations. All values are in units of the lattice constant a, and the overall time scale w_0^{-1}. For the simulation presented in Fig. 3 ($kT=0.5$), typical curvatures are of order 0.1, typical velocities of order 10^{-5}. The capillary length is about 0.1, and the anisotropy of the surface tension is 2%, which gives an anisotropy of the capillary length of 30%. Hence the order of magnitude of curvature effects is 10^{-3}. On the other hand, the coefficient β_0 is of order unity, with an anisotropy of about 30%, which for a velocity of 10^{-5} gives a kinetic anisotropy of the order 10^{-5}. Hence we conclude that kinetic effects are negligible before the anisotropy of the surface tension. This could be different for higher temperatures, where the radii of the curvature grow, and the anisotropy of the surface tension vanishes rapidly. In this case it should be difficult to detect whether static or kinetic anisotropy is the dominating effect, for they both favor the growth in the lattice diagonals.

VIII. SUMMARY

We showed that the macroscopic and mesoscopic (phase-field) equations of dendritic growth can be obtained from a microscopic master equation in a mean-field approximation. It is interesting to note that the complex pattern formation process can be obtained effectively from simple local rules. We calculated the orientation-dependent surface tension, and gave numerical results for the kinetic coefficient, finding good agreement with the standard macroscopic phenomenological theory. This approach allowed us to derive all macroscopic coefficients in terms of the microscopic interactions, which might lead to a deeper understanding of the connections between them. We believe that our model is a faithful representation of dendritic growth for small supersaturations, and when the hierarchy of length scales $a \approx \xi \ll R \ll L$ is satisfied (L is the linear system size, and R a typical radius of curvature).

The anisotropy of the surface tension is related to shape variations of the equilibrium interface: we have to include shape corrections depending on orientation. The kinetic coefficient can be derived from the shape of stationary interfaces at small velocities. Thus we see that interface structure and dynamics play key roles in the passage from microscopic to macroscopic descriptions.

The static anisotropy is a consequence of the lattice structure. In some sense, this is a trivial statement because it is well known that discretization of continuous equations leads to anisotropic behavior. The advantages of the present approach are that we can precisely quantify this effect, and that we have an underlying microscopic process which suggests that our lattice is the real crystal lattice, which evidently is also the source of anisotropy in the ''real world.''

Analyzing the possible origins of the anisotropy, we find that in the temperature domain of our simulations the needle tips are stabilized by the anisotropy of the surface tension. Thus the Gibbs-Thomson boundary condition is crucial for the formation of dendrites. This is corroborated by a comparison of our results to those of Ref. [16]: the authors used a phase-field model with a conserved phase field, coupled to a diffusion field. They integrated on a square lattice, which gives an equation of motion for the phase field very similar to ours, and yet they observed isotropic growth and formation of seaweed structures. The reason for this is that the coupling term between the phase field and the diffusion field destroyed the lattice anisotropy in their case. Therefore we see that the modification of the coupling term in phase-field

models may significantly alter the interfacial boundary conditions and the observed structures.

In summary, our model provides a method to relate macroscopic growth processes to microscopic dynamics. It allows us to investigate the interplay between microscopic interactions and macroscopic quantities intervening in the phenomenological growth equations. A serious limitation up to now has been the use of the mean-field approximation which suppresses noise. If we can devise a more careful scheme to pass from the stochastic process to the EOM, using renormalization group ideas to obtain scale-invariant equations, our approach could allow us to relate sidebranching to the equilibrium fluctuations in the bulk. This could further clarify the relations between DLA and dendritic growth.

ACKNOWLEDGMENTS

We would like to thank M. Kolb, V. Fleury, and W. Dieterich for many valuable discussions. One of us (M.P.) was supported by a grant from the Ministère de l'enseignement supérieur et de la recherche (MESR). Laboratoire de Physique de la Matière Condensée is Unité de Recherche Associée (URA) 1254 to the Centre National de la Recherche Scientifique (CNRS).

[1] D. A. Kessler, J. Koplik, and H. Levine, Adv. Phys. **37**, 255 (1988).
[2] B. Caroli, C. Caroli, B. Roulet, Y. Pomeau, and M. Ben Amar, in *Solids Far from Equilibrium*, edited by C. Godrèche (Cambridge University Press, Cambridge, 1992).
[3] E. Brener, H. Müller-Krumbhaar, and D. Temkin, Europhys. Lett. **17**, 535 (1992); T. Ihle, and H. Müller-Krumbhaar, Phys. Rev. Lett. **70**, 3083 (1993); M. Ben Amar and E. Brener, *ibid.* **71**, 589 (1993); E. Brener, *ibid.* **71**, 3653 (1993).
[4] T. A. Witten and L. M. Sander, Phys. Rev. Lett. **47**, 1400 (1981); Phys. Rev. B **27**, 5686 (1983).
[5] B. K. Johnson and R. F. Sekerka, Phys. Rev. E **52**, 6404 (1995).
[6] J. Nittmann and H. E. Stanley, J. Phys. A **20**, L981 (1987); see also H. E. Stanley, in *Fractals and Disordered Systems*, edited by A. Bunde and S. Havlin (Springer, New York, 1991).
[7] T. Vicsek, Phys. Rev. Lett. **53**, 2281 (1984).
[8] L. P. Kadanoff, J. Stat. Phys. **39**, 267 (1985); S. Liang, Phys. Rev. A **33**, 2663 (1986).
[9] J.-F. Gouyet, Europhys. Lett. **21**, 335 (1993); Phys. Rev. E **51**, 1695 (1995).
[10] K. Kawasaki, Phys. Rev. **145**, 224 (1966).
[11] P. C. Hohenberg and B. I. Halperin, Rev. Mod. Phys. **49**, 435 (1977).
[12] J. W. Cahn and J. E. Hilliard, J. Chem. Phys. **28**, 258 (1958).
[13] J. S. Langer, in *Directions in Condensed Matter Physics*, edited by G. Grinstein and G. Mazenko (World Scientific, Singapore, 1986); J. B. Collins and H. Levine, Phys. Rev. B **31**, 6119 (1985); R. Kupfermann, O. Shochet, E. Ben-Jacob, and Z. Schuss, *ibid.* **46**, 16 045 (1992).
[14] G. Caginalp and P. Fife, Phys. Rev. B **33**, 7792 (1986).
[15] A. A. Wheeler, W. J. Boettinger, and G. B. McFadden, Phys. Rev. E **47**, 1893 (1993).
[16] P. Keblinski, A. Maritan, F. Toigo, and J. R. Banavar, Phys. Rev. E **49**, 4795 (1994).
[17] W. W. Mullins and R. F. Sekerka, J. Appl. Phys. **3**, 444 (1964).
[18] M. J. Aziz and T. Kaplan, Acta Metall. **36**, 2335 (1988).
[19] M. E. Glicksmann and S. P. Marsh, in *Handbook of Crystal Growth*, edited by D. T. J. Hurle (Elsevier, Amsterdam, 1993).
[20] J. D. Gunton and M. Droz, *Introduction to the Theory of Metastable and Unstable States*, Lecture Notes in Physics Vol. 183 (Springer, New York, 1983).
[21] H. Sato and R. Kikuchi, J. Chem. Phys. **55**, 677 (1971).
[22] M. Nieswand, A. Majhofer, and W. Dieterich, Phys. Rev. E **48**, 2521 (1993); D. Reinel, W. Dieterich, and A. Majhofer, *ibid.* **50**, 4744 (1994); D. Reinel and W. Dieterich, J. Chem. Phys. **104**, 5234 (1996).
[23] J. W. Cahn, Trans. Metall. Soc. AIME **242**, 166 (1968).
[24] J. S. Langer, in *Solids Far from Equilibrium* (Ref. [2]).
[25] C. Herring, Phys. Rev. **92**, 87 (1951).
[26] M. Plapp and J.-F. Gouyet (unpublished).
[27] J. S. Langer and R. F. Sekerka, Acta Metall. **23**, 1225 (1975).